Thin Solid Films 592 (2015) 182–188

Contents lists available at ScienceDirect

Thin Solid Films

journal homepage: www.elsevier.com/locate/tsf

Conformal growth of low friction HfB_xC_y hard coatings

E. Mohimi [a], T. Ozkan [b,1], S. Babar [a], A.A. Polycarpou [b,1], J.R. Abelson [a,*]

[a] Department of Materials Science and Engineering, University of Illinois, Urbana, IL 61801, USA
[b] Department of Mechanical Science and Engineering, University of Illinois, Urbana, IL, 61801, USA

ARTICLE INFO

Article history:
Received 10 June 2015
Received in revised form 2 September 2015
Accepted 10 September 2015
Available online 12 September 2015

Keywords:
Hafnium borocarbide
CVD
Hard coating
Low friction
Conformal coating

ABSTRACT

Thin films of HfB_xC_y are deposited in a cold wall CVD apparatus using $Hf(BH_4)_4$ precursor and 3,3-dimethyl-1-butene, $(CH_3)_3CCH{=}CH_2$, as a controllable source of carbon, at substrate temperatures of 250–600 °C. As-deposited films grown at 250 °C are highly conformal (e.g., in a very deep trench, the step coverage is above 90% at a depth/width of 30:1), exhibit dense microstructure, and appear amorphous in X-ray diffraction. Increasing the carbon content from 5 to 21 at.% decreases the hardness from 21 to 9 GPa and the reduced modulus from 207 to 114 GPa. Films grown at 600 °C with carbon contents of 28 and 35 at.% exhibit enhanced hardness of 25 and 23 GPa, and reduced modulus of 211 and 202 GPa, respectively. Annealing the 300 °C grown films at 700 °C affords a nanocrystalline structure with improved mechanical properties. For films with the highest and lowest carbon contents, respectively: the coefficient of sliding friction is in the range of 0.05–0.08 and the H/E and H^3/E^2 ratios range from 0.08–0.11 and 0.15–0.40. These values indicate that C-containing films should exhibit improved wear performance in tribological applications.

1. Introduction

Conformal coatings with high hardness, low wear rates and low coefficient of friction are desirable for applications such as machines with relative motion of parts [1] and tools with re-entrant shapes [2]. Transition metal diborides and their C- or N-alloyed counterparts offer a combination of favorable tribo-mechanical properties, high chemical stability and thermal conductivity [3–10]. These films are deposited using a variety of techniques such as sputtering [6–8], chemical vapor deposition [3,11] and pulsed laser ablation [12,13]. A significant challenge is that physical vapor deposition methods lack the ability to deposit a conformal coating.

We previously reported the chemical vapor deposition (CVD) of stoichiometric, pure, and smooth HfB_2 hard coatings at substrate temperatures ≥200 °C using the halogen-free, single source precursor $Hf(BH_4)_4$. We showed that the films are extremely conformal in very high aspect ratio features, and explained this effect using a model of surface-saturated growth rate in combination with precursor transport down the depth of the feature by molecular diffusion [14,15]. We also reported the growth of Hf–B–N films by directing plasma-generated atomic nitrogen [14] or molecular ammonia to the growth surface [16].

These materials have attractive properties for tribological applications. As-deposited HfB_2 has a modulus of 340 GPa and nanoindentation hardness of 20 GPa; annealing at 700 °C transforms the structure from amorphous to nanocrystalline and raises the hardness to 40 GPa. As-deposited Hf–B–N films have somewhat reduced elastic modulus (200 GPa) and hardness (16 GPa), compared with HfB_2, and they do not crystallize upon annealing. Varying the N content or growing multilayer (HfB_2/Hf–B–N) films provides a means to tailor the overall hardness and modulus [14].

The average coefficient of friction of as deposited and annealed HfB_2 is 0.10 and 0.08, respectively, and increases to 0.18 and 0.14 after 50 passes [17]. Pin on disc experiments at high contact pressure, ~700 MPa, against AISI 440C martensitic steel showed high wear resistance of HfB_2 films. All noticeable wear was localized on the steel side and as a highly sought-after tribological quality, HfB_2 did not exhibit any measurable surface damage at all [18].

In this work, we alloy C into HfB_2 in order to enhance the tribomechanical properties of the coating expressed through a reduced coefficient of sliding friction and enhanced nanoindentation hardness, while maintaining high wear resistance. This approach is inspired and motivated by two main materials engineering and tribology considerations: firstly, aside from entirely carbon or carbon-based thin films and tribological coatings such as a-C (amorphous carbon), a-C:H (hydrogenated amorphous carbon), ta-C (tetrahedral amorphous carbon) and DLC (diamond-like carbon), introduction of elemental C into the surface of many metallic, ceramic and cermet thin film material systems has been shown to impart beneficial friction and wear properties in general [19]. Secondly, in the particular case of transition metal diborides, previous attempts to alloy C into TiB_2 coatings produced very high (or super-) hardness and improved wear properties [7]. However, Ti–B–C is typically deposited using unbalanced DC magnetron co-sputtering [6,7], a highly directional coating technique [20].

* Corresponding author.
E-mail address: abelson@illinois.edu (J.R. Abelson).
[1] Present address: Department of Mechanical Engineering, Texas A&M University, College Station, TX 77843, USA.

http://dx.doi.org/10.1016/j.tsf.2015.09.018
0040-6090/

Using CVD, we report the growth of highly conformal, low friction and wear resistant HfB_xC_y films using a halogen free process at low substrate temperature. The highly conformal nature of the process is suitable for coating complex micro- or nano-mechanical devices, vias or the interfaces of miniaturized systems that have high aspect ratio components, as well as for coating traditional tribological surfaces or parts subject to lubrication-free wear conditions at elevated temperatures.

In many CVD studies, methane (CH_4) is used as the carbon source to deposit transition metal carbide or ternary films such as HfC [11,21], TiC [22,23], and TiBC [3]. However, methane does not crack easily, which necessitates growth temperatures >800 °C [3,23] or the use of plasma decomposition [5]. In addition, the majority of metal source precursors are halogenated molecules that also require high temperature in order to react. Here, we remove these restrictions by using non-halogenated molecules — the precursor $Hf(BH_4)_4$ in combination with the olefinic carbon source 3,3-dimethyl-1-butene (DMB), $(CH_3)_3CCH{=}CH_2$. These molecules have exceptionally high vapor pressures at room temperature, 15 and 417 Torr, respectively, react at temperatures as low as 200 °C, and have efficient chemical pathways to eliminate excess atoms from the ligand groups in the form of volatile byproducts.

2. Experimental

HfB_xC_y coatings are deposited in a cold wall, high vacuum CVD chamber reported elsewhere [15,24]. Partial pressures of 0.10–0.20 mTorr for the $Hf(BH_4)_4$ precursor and 0.01–0.40 mTorr for the DMB carbon source yield different compositions of HfB_xC_y films. The substrate temperature for planar substrates is either 300 or 600 °C, and 250 °C for macrotrench and microtrench samples. Selected films are post-annealed in a tube furnace at 700 °C for 3 h in Ar gas to induce crystallization.

Si (100) is used as substrate material; it is cleaned in an ultrasonic bath for 10 min each in acetone and isopropyl alcohol, rinsed with DI water, then blown dry with nitrogen prior to loading in the chamber. The coating conformality under different growth conditions is measured using macrotrench substrates [25,26], which consist of silicon slices, 1.2 cm wide, separated by a 25 μm thick spacer on three sides. Gas transport within the macrotrench occurs in the molecular flow regime, as is the case within lithographically defined microtrench substrates, hence the kinetics that lead to conformal coating are identical. (However, the actual thickness profile is a function of the aspect ratio because the bottom of the trench introduces a boundary condition, and because microtrenches may be subject to pinch off at the opening.) The macrotrench is disassembled after film growth; precise measurements of coating thickness, composition, roughness, etc., are made as a function of depth in the trench. The conformality results are further confirmed using microtrench samples of nm-sized features.

Film microstructure and thickness are determined using cross-sectional scanning electron microscopy (SEM). Average growth rate is derived from the cross sectional SEM thickness of each film divided by the growth time. Composition and bonding are determined using X-ray photoelectron spectroscopy (XPS; PHI 5400, pass energy of 35.75 eV). ω-2θ X-ray diffraction (XRD) is used to measure the crystallinity. The adsorption of DMB and the onset of film growth are detected using in situ spectroscopic ellipsometry (SE) with photon energies in the range of 0.75–5.0 eV. Rutherford Backscattering Spectrometry (RBS) is used to calculate the atomic density of hafnium atoms by dividing the areal density obtained from RBS, by the film thickness measured from cross-sectional SEM.

The nanoindentation hardness and reduced modulus of the films are measured using a very sharp diamond indenter with tip radius of <40 nm following the Oliver–Pharr procedure [27,28]. In each loading profile, multiple loading-partial unloading (PUL) cycles are employed with increasing loads up to a maximum of 1 mN [29]. Indentation measurements are performed on films in the thickness range 150–300 nm and the maximum penetration depth of the indenter is kept to less than 10% of the film thickness to avoid substrate effects. The elastic modulus of the film E_f is calculated using the experimentally measured reduced modulus as follows:

$$\frac{1}{E_r} = \frac{1-\nu_d^2}{E_d} + \frac{1-\nu_f^2}{E_f}. \quad (1)$$

Eq. 1 assumes isotropic linearly elastic mechanical behavior for the film and indenter tip, where Poisson's ratios for diamond (ν_d) and film (ν_f) are taken as 0.07 and 0.25, respectively. The elastic modulus for the diamond tip (E_d) is 1141 GPa.

Nanoscratch experiments are performed using a conospherical diamond tip of 1 μm radius. Constant normal loads of 100, 200, 350 and 500 μN are used at a constant scratch length of 6 μm. For each film, the number of passes is continually incremented from 1 to 50 at constant 0.64 μm/s lateral tip velocity by applying successive trace and retrace motions. The coefficient of sliding friction is determined as the ratio of the measured lateral force to the applied normal load during the scratch test.

Table 1
Deposition conditions and composition for HfB_xC_y films A–F.

Sample	C (at.%)	B (at.%)	Hf (at.%)	T_{sub} (°C)	$P_{Hf(BH4)4}$ (mTorr)	P_{DMB} (mTorr)	Thick. (nm)
A	5	62	33	300	0.2	0.01	200
B	8	59	33	300	0.2	0.05	180
C	15	49	36	300	0.2	0.13	180
D	21	46	33	300	0.2	0.20	150
E	28	38	34	600	0.2	0.20	200
F	35	33	32	600	0.2	0.40	260

3. Results and discussion

3.1. HfB_xC_y film deposition

A series of growth conditions is used to prepare HfB_xC_y films of different compositions, denoted as films A to F (5–35 at.% C) (Table 1). At a $Hf(BH_4)_4$ pressure of 0.20 mTorr, substrate temperature of 300 °C, and DMB pressures of 0.01–0.2 mTorr, the film carbon content increases from 5 to 21 at.% with increasing DMB pressure. Growth ceases altogether at higher DMB pressures (discussed below), but at higher temperatures growth resumes and the films have carbon concentrations up to 35 at.%.

3.2. Growth inhibition and conformal coating

A coating will be highly conformal within a deep or complex structure, when the growth rate is kinetically limited by the reaction at the film

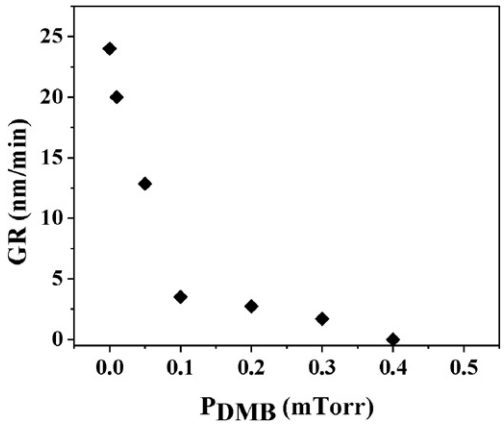

Fig. 1. Growth rate data vs. DMB pressure for HfB_xC_y samples.

surface. The introduction of a second molecular species can reduce the surface reactivity by competitive adsorption – which makes sites temporarily unavailable – or by strong chemisorption, which changes the chemical bonds available at the surface for reaction. Under these circumstances, the second species acts as a growth inhibitor [30–34]. Here, DMB not only adds carbon to the film, but also reduces the growth rate. In previous work, we determined that the HfB_2 growth rate is not fully saturated [32] using the precursor alone under the above conditions of 0.20 mTorr at 300 °C. Adding DMB at pressures of 0.01–0.30 mTorr decreases the film growth rate by 17–91%, respectively; at a pressure of 0.40 mTorr the growth rate is zero (Fig. 1). It is not possible to deduce the dominant atomic mechanism of DMB inhibition without the benefit of in-situ measurements of surface species, which is beyond the scope of this paper. However, SE provides evidence for a reduction in reactivity due to DMB absorption or reaction with the surface. (i) On a bare substrate, the incubation time for the onset of HfB_xC_y growth increases with DMB pressure. (ii) After growing a carbon-rich HfB_xC_y film, when the DMB flow is turned off, a nucleation delay of 30 s occurs before HfB_2 growth resumes using the precursor alone. Both of these observations indicate a strong reduction in reactivity due to DMB absorption or reaction with the surface. In the second experiment, if the nucleation delay is assumed to be dominated by the time required for thermal desorption of a blocking species at 250 °C, then the activation barrier is roughly 1.4 eV.

The decrease in growth rate (i.e., surface reaction rate) using DMB enhances the conformal step coverage of HfB_xC_y films. Microtrenches with aspect ratios of 0.5, 1, and 3.0 are uniformly coated using 0.2 mTorr partial pressure of each reactant at a temperature of 250 °C (Fig. 2). In panel c), filling is not quite complete – a "seam" of low density is left along the centerline. This is a consequence of the coating dynamics: as film builds up on the sidewalls, the remaining width diminishes, which increases the aspect ratio to very high values and decreases the gas transport rate by molecular diffusion [35]. We previously derived kinetic criteria that must be met to achieve seam-free filling [32,36]. Despite the seam, the results of Fig. 2 indicate that HfB_xC_y films can conformally coat structures with aspect ratios far greater than 3.

To explore the conformal coverage of very deep structures, a macrotrench sample of aspect ratio ~400 is coated with HfB_xC_y (Fig. 3). The coating thickness remains constant down to a depth/width ~30, then tapers slowly to zero at a depth/width ~160. The initial flat portion – a constant growth rate – occurs even though the partial pressures of the precursor and DMB are decreasing due to reaction on the trench walls. This behavior, along with the conformal coating profiles of Fig. 2, is evidence that the surface reaction rate is kinetically saturated, and remains so across a range of partial pressures; the growth rate starts to decrease only when the pressures fall below the values needed to maintain rate saturation. The tapering portion of the profile then results from the diffusion–reaction kinetics in this structure. Here, the aspect ratio of the trench is so large that the bottom boundary condition is zero gas pressure (zero coating rate). If instead this were a trench of aspect ratio <160, then the bottom boundary condition would be a non-zero gas pressure with only a small gradient due to reaction (film growth) on the bottom surface. Under these conditions, the gas depletion would be reduced throughout; this would both extend the depth of the plateau and reduce the slope of the profile to higher depths. It is also possible to enhance the conformality by lowering the temperature or increasing the DMB pressure to further reduce the growth rate.

At higher growth temperatures, the addition of DMB significantly improves the morphology of HfB_xC_y films. Growth of un-alloyed HfB_2

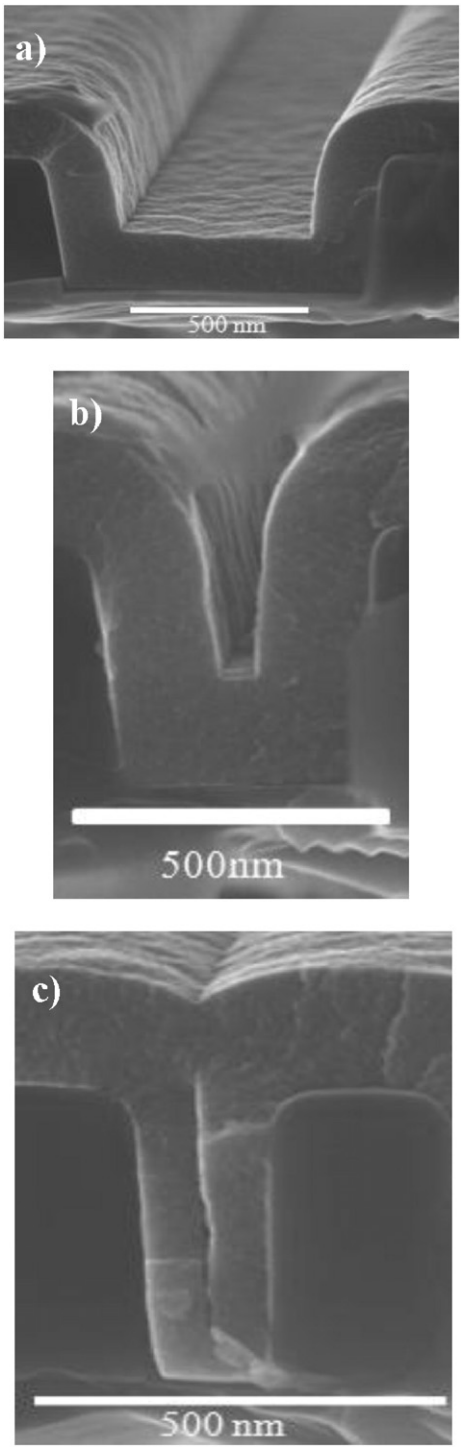

Fig. 2. a.–c. SEM images of HfB_xC_y conformal coating on microtrenches of initial aspect ratios 0.5, 1, and 3, respectively.

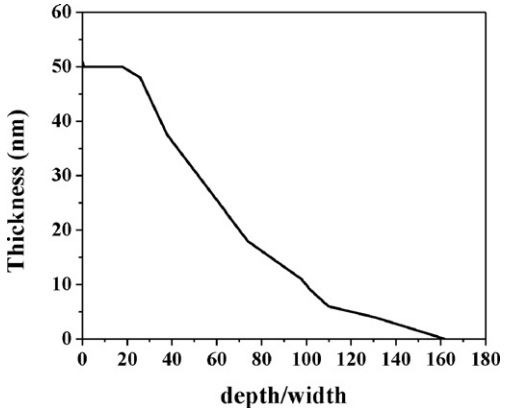

Fig. 3. Thickness profile in a macrotrench sample. Growth conditions: $T_{growth} = 250$ °C, $P_{Hf(BH_4)_4} = 0.2$ mTorr, $P_{DMB} = 0.2$ mTorr.

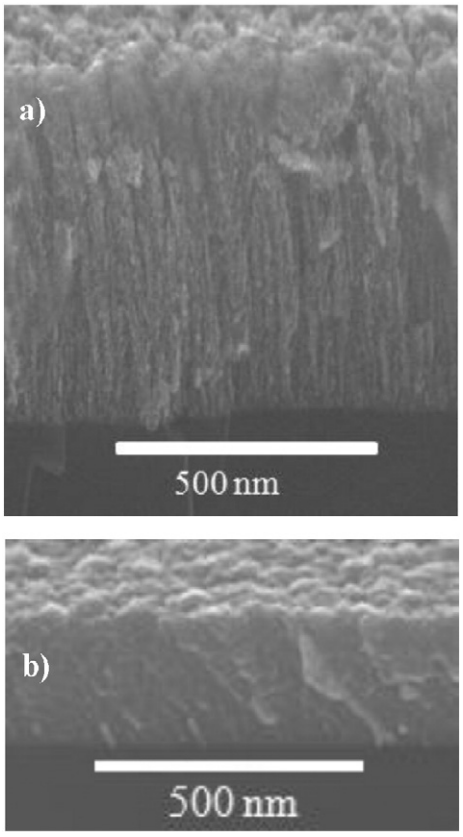

Fig. 4. Cross sectional SEM micrographs of (a) HfB_2 and (b) HfB_xC_y grown at 600 °C (sample F) on Si(100).

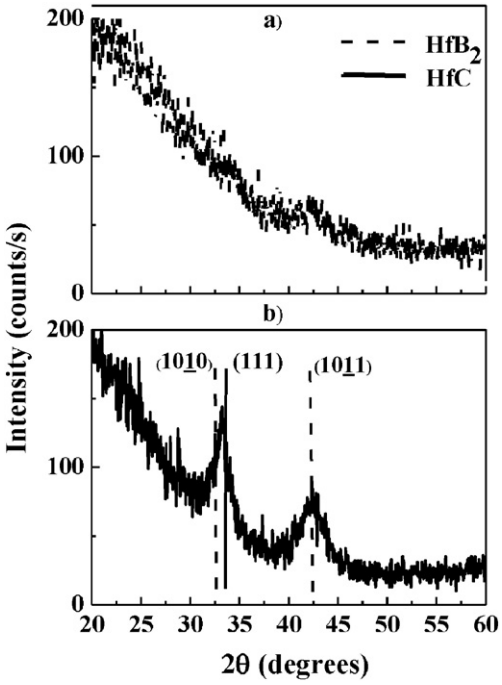

Fig. 6. XRD profiles of film A(5 at.% C) in the (a) as deposited and (b) annealed states on Si(100).

on Si(100) at 600 °C using 0.2 mTorr of $Hf(BH_4)_4$ results in a columnar film with considerable surface roughness (Fig. 4, top). Such morphology is indicative of a relatively high reaction probability of arriving precursor species. We previously showed that for high temperature HfB_2 growth, the desorption rate of surface species is high, the surface rate kinetics are far from saturation, and for this case, the effective sticking coefficient is ~0.04. However, when growth is repeated using 0.4 mTorr

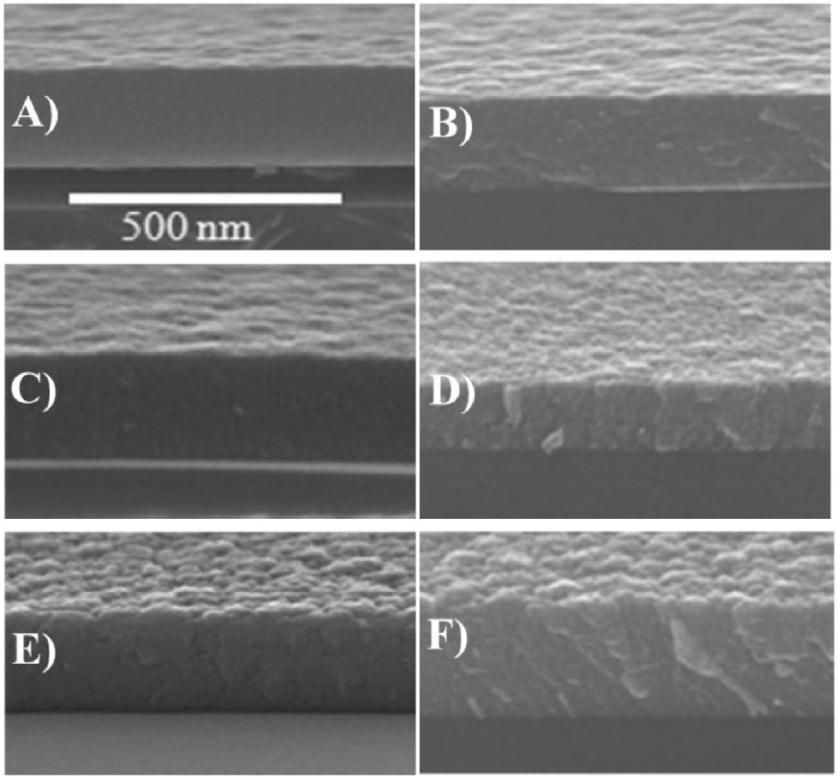

Fig. 5. Cross sectional SEM micrographs of HfB_xC_y films A–F (5–35 at.% C) grown on Si(100). The scale bar applies to all figures.

of DMB along with the precursor, the film is denser and somewhat smoother (Fig. 4, bottom). This addition of DMB reduces the surface reaction rate: film growth occurs at 60 nm/min for HfB_2 but only 26 nm/min for HfB_xC_y. A possible mechanism is the deactivation of binding (reactive) sites by C termination.

3.3. Microstructure, crystallinity and chemical composition of HfB_xC_y films

All HfB_xC_y films grown at low temperatures exhibit a dense microstructure in SEM cross sectional micrographs, and there is no apparent dependence on C content (Fig. 5). All films, including those grown at high temperature are XRD amorphous, whereas HfB_2 films grown at temperatures >400 °C are nanocrystalline [37]. HfB_xC_y films grown at low temperatures can be partly crystallized by annealing at 700 °C for 3 h under Ar atmosphere (Fig. 6). The peak positions are assigned to HfB_2 and HfC phases for films A–D (5–21 at.% C). The peak widths are broad; Scherrer analysis indicates grain sizes in the nm regime. Films grown at 600 °C and annealed at 700 °C remain amorphous; evidently the larger C content inhibits crystallization. We earlier reported that HfB_xN_y films do not crystallize when annealed to 700 °C [14].

Prior to XPS analysis, a brief sputtering (3 KV Ar^+ beam) is performed to remove surface oxygen that results from the sample transfer

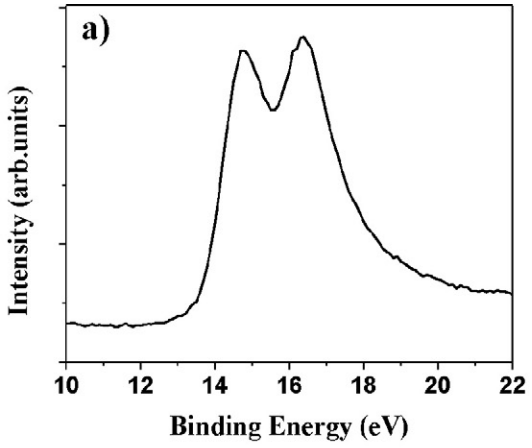

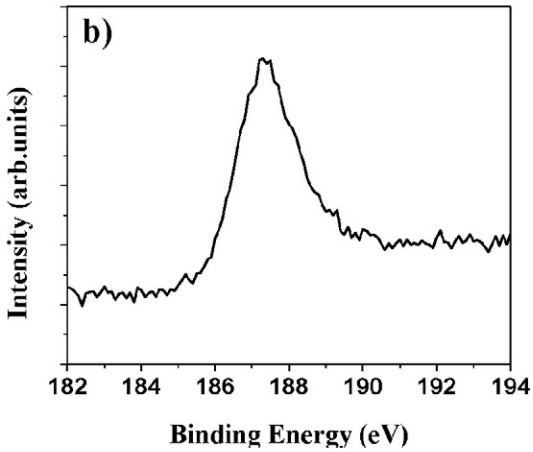

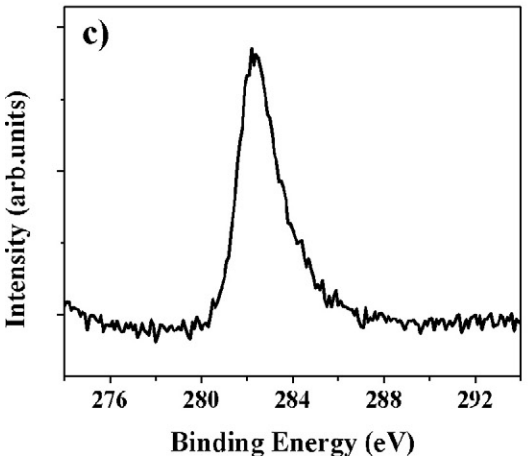

Fig. 7. XPS spectra of sample D (21 at.% C) for (a) Hf 4f (b) B 1s and (c) C 1s.

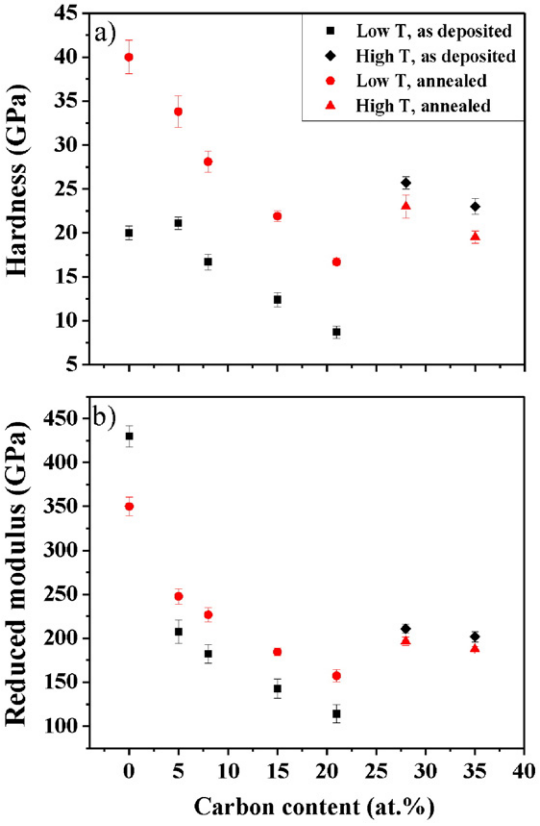

Fig. 8. Nanoindentation hardness (a) and reduced modulus (b) vs. carbon content for as deposited and annealed states of films A–F. Those with carbon >25 at.% (films E and F, diamonds and triangles) were grown at 600 °C.

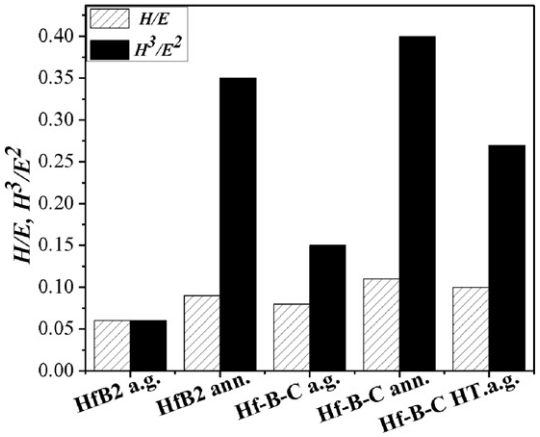

Fig. 9. Comparison of H/E and H^3/E^2 ratios for HfB_2 and HfB_xC_y films.

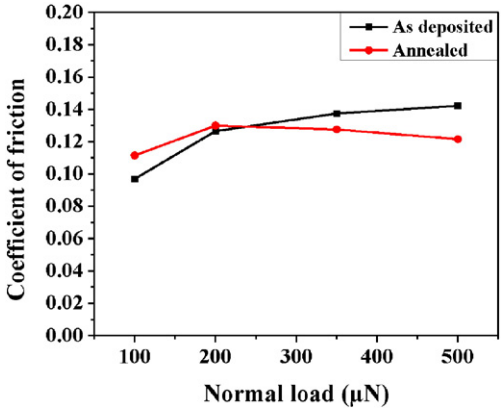

Fig. 10. Coefficient of friction for film C (15 at.% C) versus normal load for 1 pass at a sliding velocity of 0.64 μm/s.

through air. The atomic concentration of each element (Table 1) is calculated using the handbook of instrumental sensitivity factors. On the equilibrium ternary HfB_xC_y phase diagram, the film composition falls in a region bounded by the phases HfB_2, HfC, and a-C. However, at low growth temperature the material is amorphous and kinetically far from equilibrium. Films are composed of mixed bonding states; due to the proximity of the peak positions and overlaps, exact identification of bonding is not possible. For film D (21 at.% C) (Fig. 7), the peak positions for Hf 4f at 14.4 and 16.1 eV are midway between the positions for HfC_x [38] and HfB_2 [14] and no additional peak splitting or broadening is observed, which is consistent with mixed bonding on Hf sites and not with a phase segregated film. The B 1 s peak at 187.4 eV is closest to the value reported for boron in B_4C [39]. The C 1 s peak at 282.2 eV matches the value for HfC_x [38] or B_4C [39]. These data rule out the presence of a large amount of carbon precipitates. Qualitatively similar binding energy values are observed for other films in this study, and there is no obvious trend with carbon content.

3.4. Mechanical properties

The influence of carbon content is different for films grown at low temperature (300 °C) versus high temperature (600 °C). For films A to D, increasing carbon content from 5 to 21 at.% decreases the nanoindentation hardness from 21 ± 0.7 to 9 ± 0.7 GPa in the as deposited films (Fig. 8a); annealing increases the hardness, but the declining trend persists and nanoindentation hardness changes from 34 ± 1.8 to 17 ± 0.4 GPa, respectively (Fig. 8a). Annealed films have higher hardness

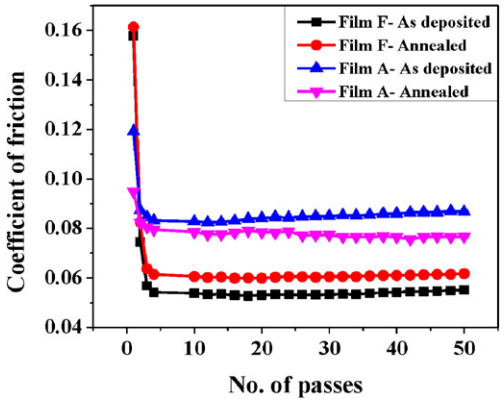

Fig. 11. Coefficient of friction versus number of passes at normal load of 500 μN and sliding velocity of 0.64 μm/s for films A (5 at.% C) and F (35 at.% C).

due to higher density and higher degree of crystallinity, as evidenced by XRD; this is similar to our previous reports for HfB_2 films [14]. Annealed HfB_xC_y films consist of a mixture of amorphous and crystalline phases; the latter presumably increase the hardness due to the presence of phase or grain boundaries and small crystalline domains within a matrix of amorphous material. The reduced moduli of these films decrease from 207 ± 13 to 114 ± 10 GPa and from 248 ± 8 to 157 ± 7 GPa for as deposited and annealed films, respectively (Fig. 8b). Similarly, taking into account the aforementioned reduced moduli, film elastic moduli calculated by virtue of Eq. (1) decrease by 50% from 237 ± 15 GPa to 119 ± 11 GPa for as deposited films with increasing carbon content, whereas for annealed films a similar drop from 296 ± 10 GPa to 171 ± 8 GPa occurs with higher amounts of carbon. Interestingly, HfB_xC_y films with 28 and 35 at.% carbon contents grown at 600 °C have the highest hardness and elastic moduli, although they are not crystalline in either the as deposited or annealed states. This behavior is attributed to the higher density of high temperature grown films as evidenced by RBS. The hafnium atomic density of Film F (35 at.% C) grown at 600 °C is 1.55×10^{22} at/cm^3, versus 1.1×10^{22} at/cm^3 for film C (15 at.% C) grown at 300 °C. For the high temperature grown films, annealing decreases the hardness and elastic modulus; this may be due to defect recovery as observed in the annealing of PVD deposited hard coatings [40]. Possibly, the hardness of high carbon content HfB_xC_y films grown at high temperatures is analogous to rapidly solidified metallic glasses that are characterized by an inherently high hardness and elastic modulus [41,42].

It is well understood that the wear resistance of a coating depends not only on hardness, but also on the level of mismatch between elastic properties of the coating and substrate. In general, a more compliant elastic response (i.e., a lower value of the elastic modulus E) defines a coating's ability to accommodate substrate strain, which increases its durability. Therefore, a high value of the H/E ratio is taken as an indication of a coating's probable resistance against impact, abrasion, erosion and sliding wear [43,44]. Another parameter, H^3/E^2, correlates well with the resistance of a film to the onset of plastic (permanent) deformation [43]. All HfB_xC_y films investigated in this work exhibit higher H/E (0.08–0.11) and H^3/E^2 ratios (0.15–0.40) compared to HfB_2 films (0.06 and 0.06, respectively). Thus the HfB_xC_y films are predicted to exhibit a high resistance to tribological wear (Fig. 9).

In 1-pass nanoscratch experiments, the coefficient of friction (COF) of film C (15 at.% C) at a constant tip velocity of 0.64 μm/s is 0.10–0.14 for the as deposited and 0.11–0.12 for the annealed film across a load range of 100–500 μN corresponding to an initial Hertzian pressure range of 7.3 GPa–14.9 GPa and stabilizes at these values at the highest loads examined (Fig. 10). Similar data are observed for other films, with a slight decrease in the COF with increasing carbon content, as expected. At a constant load of 500 μN, the COF decreases with an increasing number of passes and stabilizes at a low value of 0.08 and 0.05 for film A (lowest carbon content, 5 at.% C) and F (highest carbon content, 35 at.% C), respectively (Fig. 11). This behavior is in strong contrast to HfB_2 films, which show a steady increase in the COF with increasing number of passes. Here, the decrease in the COF with increasing number of passes is attributed to the successive transfer of loosely connected carbon within either HfB_xC_y network (i.e., matrix) or isolated a-C domains from the scar surface onto the diamond nanoscratch probe, such that the dissimilar surfaces (i.e., the tip and its scratched film counter surface) experience higher graphitic carbon content during the scratch contact as compared to their original state. Other carbon containing hard thin films such as WC, TiC and DLC have also been shown to undergo contact load and shear deformation rate dependent graphitization when subjected to pin-on-disc experiments for tribological characterization [45,46]. The governing microscopic mechanisms of this process in the particular case of HfB_xC_y thin films, conceivably also driven by high contact pressure and tribological sliding induced graphitization, is beyond the scope of this paper, but will be explored in detail in future experimental studies.

4. Conclusions

Thin films of HfB_xC_y with carbon contents of 5–35 at.% are deposited at temperatures of 250–600 °C using a halogen free precursor, $Hf(BH_4)_4$, in combination with DMB as the carbon source. As-grown films are XRD amorphous, but partially crystallize upon annealing at 700 °C for 3 h. The films contain a mixture of bonding environments similar to those in HfB_2, HfC, and B_4C. Increasing carbon content decreases the hardness and elastic modulus of low-temperature deposited films; however, HfB_xC_y films have higher H/E and H^3/E^2 ratios than for HfB_2, which is predicted to improve the wear performance in tribological applications. The use of DMB retards the film growth rate and enhances the conformal coating of HfB_xC_y within deep trenches, including high aspect ratio structures. Nanoscratch tests indicate ultra-low coefficient of friction values, 0.05, at higher carbon content values. Together, these results indicate that HfB_xC_y coatings are highly suitable for tribological applications.

Acknowledgments

This research was supported by the National Science Foundation under grant no. NSF CMMI 1030657. Compositional and structural analyses of films were carried out in part in the Frederick Seitz Materials Research Laboratory Central Research Facilities, University of Illinois. Authors gratefully acknowledge the help of Dr. Kathy Walsh with nanoscratch tests and Hysitron TI-950 TriboIndenter operation. Authors gratefully acknowledge Professor G. S. Girolami and P. Sempsrott in the Department of Chemistry at University of Illinois Urbana Champaign for precursor design and synthesis.

References

[1] N. Rajan, C.A. Zorman, M. Mehregany, R. DeAnna, R.J. Harvey, Effect of MEMS-compatible thin film hard coatings on the erosion resistance of silicon micromachined atomizers, Surf. Coat. Technol. 108 (1–3) (1998) 391.
[2] C. Mitterer, F. Holler, D. Reitberger, E. Badisch, M. Stoiber, C. Lugmair, R. Nobauer, T. Muller, R. Kullmer, Industrial applications of PACVD hard coatings, Surf. Coat. Technol. 163 (2003) 716.
[3] H. Holzschuh, Chemical-vapor deposition of wear resistant hard coatings in the Ti–B–C–N system: properties and metal-cutting tests, Int. J. Refract. Met. Hard Mater. 20 (2) (2002) 143.
[4] H. Karner, J. Laimer, H. Stori, P. Rodhammer, Preparation of TiB_2 and TiB_xN_y coatings by PACVD, Surf. Coat. Technol. 39 (1–3) (1989) 293.
[5] C. Mitterer, F. Holler, C. Lugmair, R. Nobauer, R. Kullmer, C. Teichert, Optimization of plasma-assisted chemical vapour deposition hard coatings for their application in aluminium die-casting, Surf. Coat. Technol. 142 (2001) 1005.
[6] C. Mitterer, P.H. Mayrhofer, M. Beschliesser, P. Losbichler, P. Warbichler, F. Hofer, P.N. Gibson, W. Gissler, H. Hruby, J. Musil, J. Vlcek, Microstructure and properties of nanocomposite Ti–B–N and Ti–B–C coatings, Surf. Coat. Technol. 120 (1999) 405.
[7] C. Mitterer, M. Rauter, P. Rodhammer, Sputter deposition of ultrahard coatings within the system TI–B–C–N, Surf. Coat. Technol. 41 (3) (1990) 351.
[8] P.H. Mayrhofer, G. Tischler, C. Mitterer, Microstructure and mechanical/thermal properties of Cr–N coatings deposited by reactive unbalanced magnetron sputtering, Surf. Coat. Technol. 142 (2001) 78.
[9] H. Willmann, P.H. Mayrhofer, P.O.A. Persson, A.E. Reiter, L. Hultman, C. Mitterer, Thermal stability of Al–Cr–N hard coatings, Scr. Mater. 54 (11) (2006) 1847.
[10] P.H. Mayrhofer, C. Mitterer, High-temperature properties of nanocomposite TiB_xN_y and TiB_xC_y coatings, Surf. Coat. Technol. 133 (2000) 131.
[11] Y.L. Wang, X. Xiong, G.D. Li, X.J. Zhao, Z.K. Chen, W. Sun, Z.S. Wang, Effect of gas composition on the microstructure and growth behavior of HfC coatings prepared by LPCVD, Solid State Sciences 20 86.
[12] R. Teghil, A. Santagata, M. Zaccagnino, S.M. Barinov, V. Marotta, G. De Maria, Hafnium carbide hard coatings produced by pulsed laser ablation and deposition, Surf. Coat. Technol. 151 (2002) 531.
[13] D. Ferro, J.V. Rau, V.R. Albertini, A. Generosi, R. Teghil, S.M. Barinov, Pulsed laser deposited hard TiC, ZrC, HfC and TaC films on titanium: hardness and an energy-dispersive X-ray diffraction study, Surf. Coat. Technol. 202 (8) (2008) 1455.
[14] S. Jayaraman, J.E. Gerbi, Y. Yang, D.Y. Kim, A. Chatterjee, P. Bellon, G.S. Girolami, J.P. Chevalier, J.R. Abelson, HfB_2 and Hf–B–N hard coatings by chemical vapor deposition, Surf. Coat. Technol. 200 (22–23) (2006) 6629.
[15] S. Jayaraman, Y. Yang, D.Y. Kim, G.S. Girolami, J.R. Abelson, Hafnium diboride thin films by chemical vapor deposition from a single source precursor, J. Vac. Sci. Technol. A 23 (6) (2005) 1619.
[16] N. Kumar, W. Noh, S.R. Daly, G.S. Girolami, J.R. Abelson, Low temperature chemical vapor deposition of hafnium nitride–boron nitride nanocomposite films, Chem. Mater. 21 (23) (2009) 5601.
[17] A. Chatterjee, N. Kumar, J.R. Abelson, P. Bellon, A.A. Polycarpou, Nanoscratch and nanofriction behavior of hafnium diboride thin films, Wear 265 (5–6) (2008) 921.
[18] A. Chatterjee, S. Jayaraman, J.E. Gerbi, N. Kumar, J.R. Abelson, P. Bellon, A.A. Polycarpou, J.P. Chevalier, Tribological behavior of hafnium diboride thin films, Surf. Coat. Technol. 201 (7) (2006) 4317.
[19] K. Holmberg, A. Matthews, Coatings Tribology, Properties, Mechanisms, Techniques and Applications in Surface Engineering, Elsevier, Amsterdam, the Netherlands, 2009.
[20] S. Mahieu, K. Van Aeken, D. Depla, D. Smeets, A. Vantomme, Dependence of the sticking coefficient of sputtered atoms on the target-substrate distance, J. Phys. D. Appl. Phys. 41 (15) (2008) 4.
[21] Y.L. Wang, X. Xiong, G.D. Li, H.B. Zhang, Z.K. Chen, W. Sun, X.J. Zhao, Microstructure and ablation behavior of hafnium carbide coating for carbon/carbon composites, Surf. Coat. Technol. 206 (11–12) (2012) 2825.
[22] T. Takeuchi, H. Miyoshi, Y. Egashira, H. Komiyama, Chemical vapor deposition of silicon carbide titanium carbide composite films from dichlorodimethylsilane, titanium tetrachloride, and methane, J. Electrochem. Soc. 146 (2) (1999) 564.
[23] C. Bisch, M. Nadal, F. Teyssandier, M. Bancel, B. Vallon, Chemical-vapor-deposition of titanium carbide on WC–Co cemented carbides, Mater. Sci. Eng., A 202 (1–2) (1995) 238.
[24] S. Jayaraman, E.J. Klein, Y. Yang, D.Y. Kim, G.S. Girolami, J.R. Abelson, Chromium diboride thin films by low temperature chemical vapor deposition, J. Vac. Sci. Technol. A 23 (4) (2005) 631.
[25] A. Nuruddin, J.R. Doyle, J.R. Abelson, Surface-reaction probability in hydrogenated amorphous-silicon growth, J. Appl. Phys. 76 (5) (1994) 3123.
[26] Y. Yang, S. Jayaraman, D.Y. Kim, G.S. Girolami, J.R. Abelson, CVD growth kinetics of HfB_2 thin films from the single-source precursor $Hf(BH_4)_4$, Chem. Mater. 18 (21) (2006) 5088.
[27] W.C. Oliver, G.M. Pharr, An improved technique for determining hardness and elastic-modulus using load and displacement sensing indentation experiments, J. Mater. Res. 7 (6) (1992) 1564.
[28] W.C. Oliver, G.M. Pharr, Measurement of hardness and elastic modulus by instrumented indentation: advances in understanding and refinements to methodology, J. Mater. Res. 19 (1) (2004) 3.
[29] H.S. Seo, T.Y. Lee, J.G. Wen, I. Petrov, J.E. Greene, D. Gall, Growth and physical properties of epitaxial HfN layers on MgO(001), J. Appl. Phys. 96 (1) (2004) 878.
[30] N. Kumar, A. Yanguas-Gil, S.R. Daly, G.S. Girolami, J.R. Abelson, Growth inhibition to enhance conformal coverage in thin film chemical vapor deposition, J. Am. Chem. Soc. 130 (52) (2008) 17660.
[31] A. Yanguas-Gil, N. Kumar, Y. Yang, J.R. Abelson, Highly conformal film growth by chemical vapor deposition. II. Conformality enhancement through growth inhibition, J. Vac. Sci. Technol. A 27 (5) (2009) 1244.
[32] A. Yanguas-Gil, Y. Yang, N. Kumar, J.R. Abelson, Highly conformal film growth by chemical vapor deposition. I. A conformal zone diagram based on kinetics, J. Vac. Sci. Technol. A 27 (5) (2009) 1235.
[33] S. Babar, L.M. Davis, P. Zhang, E. Mohimi, G.S. Girolami, J.R. Abelson, Chemical vapor deposition of copper: use of a molecular inhibitor to afford uniform nanoislands or smooth films, ECS J. Solid State Sci. Technol. 3 (5) (2014) Q79.
[34] S. Babar, N. Kumar, P. Zhang, J.R. Abelson, Growth inhibitor to homogenize nucleation and obtain smooth HfB_2 thin films by chemical vapor deposition, Chem. Mater. 25 (5) (2013) 662.
[35] C. Chang, T. Abe, M. Esashi, Trench filling characteristics of low stress TEOS/ozone oxide deposited by PECVD and SACVD, Microsyst. Technol. 10 (2) (2004) 97.
[36] W.B. Wang, N.N. Chang, T.A. Codding, G.S. Girolami, J.R. Abelson, Superconformal chemical vapor deposition of thin films in deep features, J. Vac. Sci. Technol. A 32 (5) (2014).
[37] Y. Yang, S. Jayaraman, D.Y. Kim, G.S. Girolami, J.R. Abelson, Crystalline texture in hafnium diboride thin films grown by chemical vapor deposition, J. Cryst. Growth 294 (2) (2006) 389.
[38] G.R. Gruzalski, D.M. Zehner, Charge-distribution changes accompanying the formation and changes in the composition of HfC_X and TaC_X, Phys. Rev. B 42 (5) (1990) 2768.
[39] L.G. Jacobsohn, R.K. Schulze, M. da Costa, M. Nastasi, X-ray photoelectron spectroscopy investigation of boron carbide films deposited by sputtering, 572 (2–3) (2004) 418–Surf. Sci.
[40] P.H. Mayrhofer, C. Mitterer, L. Hultman, H. Clemens, Microstructural design of hard coatings, Prog. Mater. Sci. 51 (8) (2006) 1032.
[41] M. Ohtsuki, R. Tamura, S. Takeuchi, S. Yoda, T. Ohmura, Hard metallic glass of tungsten-based alloy, Appl. Phys. Lett. 84 (24) (2004) 4911.
[42] M. Ohtsuki, K. Nagata, R. Tamura, S. Takeuchi, Tungsten-based metallic glasses with high crystallization temperature, high modulus and high hardness, Mater. Trans. 46 (1) (2005) 48.
[43] A. Leyland, A. Matthews, On the significance of the H/E ratio in wear control: a nanocomposite coating approach to optimised tribological behaviour, Wear 246 (1–2) (2000) 1.
[44] A. Leyland, A. Matthews, Design criteria for wear-resistant nanostructured and glassy-metal, Surf. Coat. Technol. 177 (2004) 317.
[45] Y. Liu, A. Erdemir, E.I. Meletis, An investigation of the relationship between graphitization and frictional behavior of DLC coatings, Surf. Coat. Technol. 86–7 (1–3) (1996) 564.
[46] A.A. Voevodin, J.S. Zabinski, Supertough wear-resistant coatings with 'chameleon' surface adaptation, Thin Solid Films 370 (1–2) (2000) 223.